First estimates of the contribution of CaCO$_3$ precipitation to the release of CO$_2$ to the atmosphere during young sea ice growth

N.-X. Geilfus,[1,2,3] G. Carnat,[3] G. S. Dieckmann,[4] N. Halden,[3] G. Nehrke,[4] T. Papakyriakou,[3] J.-L. Tison,[2] and B. Delille[1]

[1] We report measurements of pH, total alkalinity, air-ice CO$_2$ fluxes (chamber method), and CaCO$_3$ content of frost flowers (FF) and thin landfast sea ice. As the temperature decreases, concentration of solutes in the brine skim increases. Along this gradual concentration process, some salts reach their solubility threshold and start precipitating. The precipitation of ikaite (CaCO$_3$.6H$_2$O) was confirmed in the FF and throughout the ice by Raman spectroscopy and X-ray analysis. The amount of ikaite precipitated was estimated to be 25 µmol kg^{-1} melted FF, in the FF and is shown to decrease from 19 to 15 µmol kg^{-1} melted ice in the upper part and at the bottom of the ice, respectively. CO$_2$ release due to precipitation of CaCO$_3$ is estimated to be 50 µmol kg^{-1} melted samples. The dissolved inorganic carbon (DIC) normalized to a salinity of 10 exhibits significant depletion in the upper layer of the ice and in the FF. This DIC loss is estimated to be 2069 µmol kg^{-1} melted sample and corresponds to a CO$_2$ release from the ice to the atmosphere ranging from 20 to 40 mmol m^{-2} d^{-1}. This estimate is consistent with flux measurements of air-ice CO$_2$ exchange. Our measurements confirm previous laboratory findings that growing young sea ice acts as a source of CO$_2$ to the atmosphere. CaCO$_3$ precipitation during early ice growth appears to promote the release of CO$_2$ to the atmosphere; however, its contribution to the overall release by newly formed ice is most likely minor.

1. Introduction

[2] Most carbon cycle research has not considered the possibility of either direct air-sea gas exchange in the presence of sea ice or indirect air-ice-ocean gas exchange, where sea ice plays an active role in CO$_2$ transfer. Global and regional budgets of air-sea CO$_2$ exchange have ignored ice-covered regions [*Bates and Mathis*, 2009; *Takahashi et al.*, 2009], relying instead on the assumption that a sea ice cover is impermeable to gases. However, recent observations using both tower-based micrometeorological approaches and chamber sampling indicate that uptake and evasion of CO$_2$ does occur over sea ice [*Semiletov et al.*, 2004; *Delille*, 2006; *Zemmelink et al.*, 2006; *Semiletov et al.*, 2007; *Nomura et al.*, 2010b; *Nomura et al.*, 2010a; *Miller et al.*, 2011; *Papakyriakou and Miller*, 2011]. Observations of gas exchange have been attributed to numerous processes in sea ice, both physiochemical and biological, but the community is uncertain of the amount of CO$_2$ that sea ice can exchange with the atmosphere and ocean, as well as the overall role played by sea ice as a sink or source of CO$_2$ to the atmosphere. In addition, current observations of gas exchanges vary by several orders of magnitude depending on the method. Fluxes reported by the chamber method [*Delille et al.*, 2007; *Nomura et al.*, 2010b; *Nomura et al.*, 2010a; *Geilfus et al.*, 2012] are significantly lower than fluxes measured by eddy covariance [*Semiletov et al.*, 2004; *Zemmelink et al.*, 2006; *Miller et al.*, 2011; *Papakyriakou and Miller*, 2011]. *Semiletov et al.* [2004] reported that melt ponds and open brine channels within sea ice represent a sink for atmospheric CO$_2$, of up to -39.3 mmol m^{-2} d^{-1}. *Papakyriakou and Miller* [2011] observed CO$_2$ fluxes over seasonal sea ice in the Canadian Arctic Archipelago to be highly variable, with

[1]Unité d'Océanographie Chimique, Université de Liège, Liège, Belgium.

[2]Laboratoire de Glaciologie, DSTE, Université Libre de Bruxelles, Brussels, Belgium.

[3]Center of Earth Observation Science, University of Manitoba, Winnipeg, Manitoba, Canada.

[4]Biogeosciences, Alfred Wegener Institute for Polar and Marine Research, Bremerhaven, Germany.

Corresponding author: N.-X. Geilfus, Center for Earth Observation Science, University of Manitoba, 496 Wallace Bldg, 125 Dysart Road, Winnipeg, MB R3T 2N2, Canada. (Nicolas-Xavier.Geilfus@ad.umanitoba.ca)

hourly peak exchanges ranging from $+86.4$ down to -259 mmol m^{-2} d^{-1}, during cold and warm phases (respectively) of the spring transition. The large but short-lived late-spring spike in sea ice uptake of atmospheric CO_2 corresponds in time to increased sea ice permeability and a corresponding rapid increase in brine volume associated with opening of brine channels, leading the authors to speculate that the downward flux was driven in part by photosynthesis at the ice base. Using the chamber method, *Delille* [2006] measured CO_2 fluxes, ranging from -4 to $+2$ mmol m^{-2} d^{-1} over Antarctic pack ice, and related these fluxes to the seasonal differences in brine pCO_2 relative to the atmospheric concentration. *Nomura et al.* [2010b] also measured CO_2 fluxes ranging from -1 to $+0.7$ mmol m^{-2} d^{-1} using chambers over warming first year land-fast sea ice in Barrow in the late spring. *Delille* [2006] and *Nomura et al.* [2010b] ascribed the flux direction to the difference in air-sea ice brine pCO_2.

[3] The studies outlined above document fluxes over mature, slow-growing or decaying seasonal sea ice. Fluxes over growing artificial sea ice have been reported by *Nomura et al.* [2006], however comparative field measurements of fluxes over thin, rapidly growing sea ice do not exist. This represents a significant gap in our understanding of CO_2 exchange over the annual growth/decay sea ice cycle.

[4] As mentioned, uncertainty remains regarding the exact drivers of the CO_2 exchange across the air-sea ice-ocean interface, although several potential processes have been identified. As sea ice forms and grows thicker, salts are partly rejected from the sea ice and partly trapped within the sea ice structure, concentrated into brine pockets, tubes, and channels in the sea ice [*Weeks and Ackley*, 1982]. A reduction in the brine temperature promotes increased brine salinity and concentration of solutes (including DIC) and increased brine pCO_2 through a decrease in brine CO_2 solubility [*Papadimitriou et al.*, 2004]. Significant changes in the mineral-liquid thermodynamic equilibrium can occur with changes in temperature, leading to sequential mineral precipitation [*Marion*, 2001]. Ikaite, a hexahydrate polymorph of calcium carbonate ($CaCO_3 \cdot 6H_2O$), begins to precipitate at $-2.2\,°C$ and mirabilite ($Na_2SO_4 \cdot 10H_2O$) below $-8\,°C$. $NaCl \cdot 2H_2O$ precipitates below $-26\,°C$, while potassium and magnesium salts precipitate below $-34\,°C$ [*Assur*, 1958; *Rankin et al.*, 2000; *Marion*, 2001]. The precipitation of calcium carbonate from the brine [*Papadimitriou et al.*, 2004; 2008; *Dieckmann et al.*, 2008, 2010] also increases the brine pCO_2. Sea ice hosts a complex biological system [*Thomas et al.*, 2010] and carbon is cycled through the processes of photosynthesis and respiration associated with seasonally large algal communities [*Arrigo et al.*, 2010] and bacterial communities that are thought to function throughout the annual cycle [*Deming*, 2010]. CO_2 can be exchanged among sea ice brine, seawater, and atmosphere, as long as the ice remains permeable [*Nomura et al.*, 2006; *Rysgaard et al.*, 2007; *Loose et al.*, 2009].

[5] The possible role of $CaCO_3$ precipitation on sea ice carbonate biochemistry has received growing attention. *Rysgaard et al.* [2007; 2009] suggested that calcium carbonate precipitation in sea ice could act as a significant sink for atmospheric CO_2. An abiotic pump would result from the high DIC : TA - ratio (TA being defined as the total alkalinity) of brine expelled from sea ice during the ice growth and brine drainage as a consequence of $CaCO_3$ precipitation, which is described by

$$2HCO_3^- + Ca^{2+} \leftrightarrow CaCO_3 + H_2O + CO_2. \qquad (1)$$
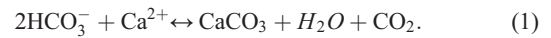
[6] Precipitation of 1 mol of $CaCO_3$ transfers HCO_3^- to the CO_2 pool, decreasing DIC by 1 mol and TA by 2 mol. According to *Rysgaard et al.* [2007], this pump could represent a downward transport of 0.2–0.5 Pg C y^{-1} out of the surface ocean. However, the role and significance of $CaCO_3$ formation/dissolution in sea ice on atmospheric CO_2 depend on the rate of mineral production and sea ice permeability; the latter depending on the conditions and timing of precipitation and the fate of the precipitate [*Delille*, 2006].

[7] The authigenesis of ikaite in natural sea ice is not yet fully understood. Little is known about the spatial and temporal occurrence of ikaite precipitates in sea ice, but recent discovery of ikaite in sea ice at both poles indicates that ikaite precipitation is not a localized phenomenon [*Dieckmann et al.*, 2008; 2010]. Ikaite stability is limited to near-freezing temperatures and is apparently favored by alkaline conditions, elevated phosphate concentrations, and by the presence of certain additives like amino acids [*J. L. Bischoff et al.*, 1993a; *Whiticar and Suess*, 1998; *Buchardt et al.*, 2001; *Selleck et al.*, 2007].

[8] In addition to the abiotic pump suggested by *Rysgaard et al.*, [2007; 2009], $CaCO_3$ precipitation at the top of sea ice is thought to play a role in atmospheric chemistry as a trigger for the transformation of inert sea-salt bromide to reactive bromine monoxide and the occurrence of tropospheric ozone depletion events (ODEs) at high latitudes [*Sander et al.*, 2006]. It was suggested that this conversion was possibly due to an alkalinity decrease [*Sander et al.*, 2006]. However, *Morin et al.* [2008] pointed out that the alkalinity decrease required for such transformation may not occur in sea ice and that further work is needed to resolve this issue. *Piot and von Glasow* [2008] showed that the precipitation of calcium carbonate ($CaCO_3$) in sea ice brine is a key process allowing for the rapid acidification of aerosols originating from frost flowers (FF), highlighting the potential importance of FF for ozone chemistry in the Arctic. Their work supports earlier suggestions that FF and their accompanying brine skim (BS) may play an important role as a source of salt aerosols for the atmosphere [*Rankin et al.*, 2000; 2002; *Alvarez-Aviles et al.*, 2008]. FF mainly grow on newly formed sea ice [*Perovich and Richter-Menge*, 1994; *Alvarez-Aviles et al.*, 2008] and are centimeter-scale ice structures, formed by a mixture of atmospheric hoar and liquid from the BS, brine expelled from the ice crystals during the sea ice growth. The latter explains the observed high bulk salinity of FF. Growth is thought to proceed in three stages [*Alvarez-Aviles et al.*, 2008]: (i) development of small nodules on nilas, (ii) the initial formation of FF on the nodules, and (iii) their subsequent growth into mature structures.

[9] To the best of our knowledge, field measurements of CO_2-related parameters have not yet been reported over young, rapidly forming sea ice; laboratory experiments suggest that young newly formed sea ice releases CO_2 to the atmosphere [*Nomura et al.*, 2006]. During fieldwork in Barrow (Alaska) in 2009, we had the opportunity to sample a newly formed ice sheet and associated FF. In this paper, quantitative analysis of pH, TA, and amount of ikaite precipitates in FF and bulk sea ice identified the influence of an abiotic process on the sea ice carbonate system during the

early growth phase and to demonstrate calcium carbonate precipitation as ikaite. Furthermore, we report the first Arctic measurements of air-sea CO$_2$ fluxes over young growing ice and FF and provide a first assessment of the contribution of CaCO$_3$ precipitation to the total observed CO$_2$ release to the atmosphere from those media.

2. Methods

[10] Individual FF, surface BS, and young sea ice cores (20 cm thick) were collected from young shore-fast sea ice near Barrow, Alaska, on 6 April 2009 (Figure 1). A half dozen FF were sampled by scrapping the ice surface using a clean spatula and were stored frozen in a clean plastic bag. A Teflon-coated stainless steel ice corer with an internal diameter of 7 cm was used to sample a total of five cores from the young ice in an area of 1 m^2 with a maximum spacing between cores of 20 cm. Sea ice temperature was measured in situ directly after extraction of the first core, using a calibrated probe (TESTO 720) inserted in pre-drilled holes (perpendicular to the vertical in the side of the core) at the exact diameter of the probe and with a depth resolution of 2.5 cm in the vertical with $\pm 0.1\,^\circ$C precision (not including potential bias from the heat transfer during drilling or temperature change during temperature measurements). Sea ice cores and FF samples were stored on the sampling site in an isolated box filled with individual cooling bags, pre-cooled at $-30\,^\circ$C. Back in the lab, samples were kept

frozen at $-28\,^\circ$C. In the lab, the temperature core was cut into successive 2.5 cm thick slices. Each slice was stored in a bucket and left to melt at $+4\,^\circ$C in the dark. Salinity of the melt water was measured with a Thermo-Orion$^\circledR$ portable salinometer WP-84TPS meter with a precision of ± 0.1. The brine volume fraction was calculated using the equations given by *Eicken* [2003] and references therein.

[11] Vertical thin sections were performed on one of the cores following standard procedures [*Tison et al.*, 2008], in order to describe the texture of the ice. Pictures of crystal texture were taken of the thin sections using a light table and cross- and parallel-polarized sheets with a macro setting on a camera (Nikon$^\circledR$ Coolpix S200, 7.1 megapixels).

[12] Another core was cut into vertical sections at a 5 cm depth resolution. From each section, 20 g of ice was melted at room temperature to measure phosphate using standard colorimetric procedure on a Genesys$^\circledR$ spectrophotometer [*Grasshoff et al.*, 1983].

[13] Fluxes of CO$_2$ at the sea ice-atmosphere interface were measured using an accumulation chamber (West System$^\circledR$) at four places over the sampling site in an area of 2 m^2. The chamber is a metal cylinder closed at the top, with an internal diameter of 20 cm and an internal height of 9.7 cm. A rubber seal surrounded by a serrated metal edge ensured an airtight connection between the ice and the accumulation chamber. The chamber was connected in a closed loop to an infrared gas analyzer (Licor$^\circledR$ 6262) using an air pump set at 3 L min^{-1}. The measurement of pCO$_2$ in the chamber was recorded every
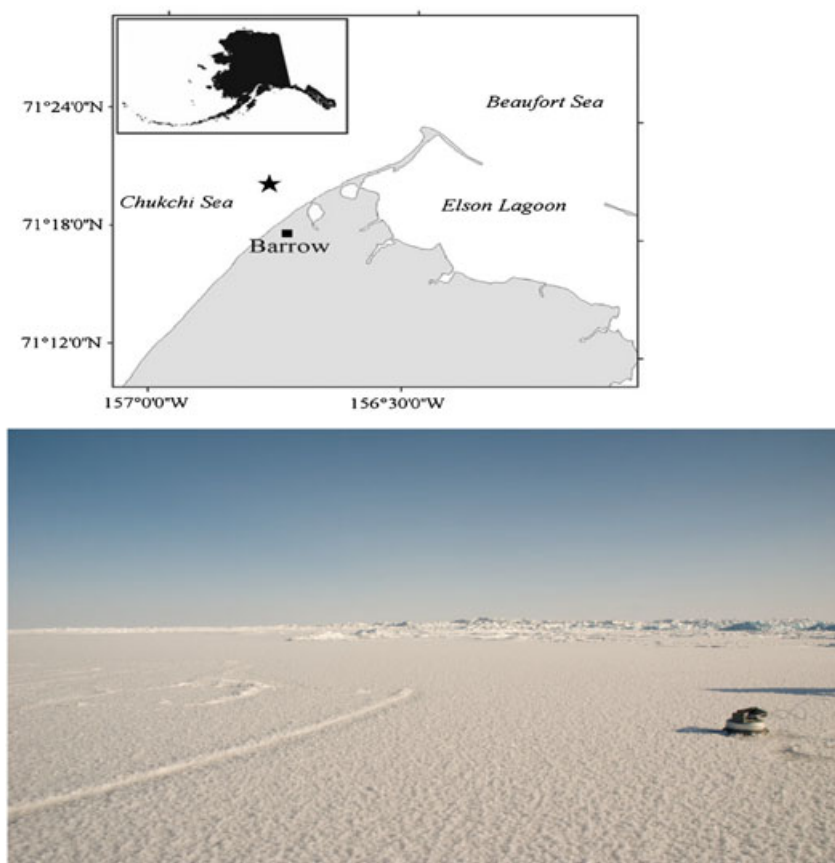

Figure 1. Location of the sampling area (black star) at Barrow, Alaska, and pictures of the sampling site. The chamber of accumulation is 20 cm of diameter.

30 s for a minimum of 5 min. The flux was then computed from the slope of the linear regression of pCO$_2$ against time ($r^2 > 0.99$) according to *Frankignoulle* [1988]. Uncertainty of the flux computation due to the standard error on the regression slope was $\pm 3\%$ on average.

[14] Crystals of calcium carbonate were extracted from the ice cores following *Dieckmann et al.* [2008]. Ice cores were cut into 5 cm sections, which were then transferred into clean plastic containers, sealed, and melted at +4 °C. Samples were processed as soon as they were melted. Melt water temperature never rose significantly above 0 °C. The melt water was gently swirled so most of the crystals settled in the central part of the container. Using the first ice core, a proportion of the crystals were collected for direct observation under a binocular microscope, while the rest of the crystals were stored on 0.2 μm Millipore filters which were rinsed with 75% ethanol and kept frozen at −25 °C for later identification of the mineralogical phase. On a twin ice core, the same melting process was followed but the crystals were pipetted into a glass vial containing 60% ethanol and kept frozen at −18 °C for the identification of the mineralogical phase.

[15] Crystal identification was carried out by X-ray diffraction using a Siemens® (Bruker) D5000 Powder Diffractometer at room temperature. Bruker's DIFFRAC-plus software and MDI Jade+ software were used to collect and analyze the data. The goniometer was configured in Bragg-Brentano (θ-2θ) geometry and used Cu radiation (Cu Kα1 $\lambda = 1.54060$). The system was equipped with computer-controlled divergence and receiving slits, a rotating sample holder, diffracted beam graphite monochromator, and a scintillation detector. Scanning electron microscopy (SEM) was performed on a single crystal, from the same filter used for the X-ray (left 1 day at room temperature). The instrument used was a Cambridge® Stereoscan 120, running at 20 keV. Others analyses using a confocal Raman microscope (WITec®, Ulm, Germany) were performed for phase identification of the crystals extracted. The Raman was equipped with a diode laser (532 nm) and an Olympus® 20x Teflon coated water objective. The sample was transferred in a temperature-controlled room into cooled (~ 1 °C) glass Petri dishes and transferred to the Raman microscope. The ikaite stayed stable for at least 15 min with this approach, before signs of transformation into calcite were observed. Time was sufficient for reliable phase identification of ikaite given that the measurement took only a few seconds.

[16] The size of CaCO$_3$ crystals found in our sample ranged from <40 μm to 200 μm (Fig. 2), so they could all be removed by filtration on 0.2 μm filters. According to previous work of *Rysgaard et al.* [2007] and [2009], we assumed that dissolution of CaCO$_3$ crystals during the melting process was not significant, and attention was paid to keep the sample below +4 °C at all time during melting process, filtration, and pH measurement. The overall calcium carbonate content (ΔCaCO$_3$) was then estimated from the difference between the alkalinity of unfiltered sample, denoted as bulk alkalinity (TA_b) and the sample filtered on 0.2 μm Millipore filters, denoted as filtered alkalinity (TA_f). ΔCaCO$_3$ is computed according to

$$\Delta \text{CaCO}_3 = \frac{1}{2}\left(TA_b - TA_f\right). \tag{2}$$

[17] Ice cores and FF were then melted and processed according to the following methodology in order to estimate the amount of precipitated CaCO$_3$. Twin ice cores, cut into 5 cm segments, and FF were transferred into Tedlar® gas sampling bags, closed with a 30 cm gas-tight Tygon tube. The excess air was quickly removed through the valve. The ice samples were melted in a fridge at +4 °C. As soon as the ice was completely melted, samples were collected to measure pH, TA_b, and TA_f. The melt water was shaken, re-suspending the crystals and leaving the liquid homogenized. First, samples for TA_b were collected, then samples for TA_f. The filtration was carried out at +4 °C to avoid any calcium carbonate dissolution. Then, pH was measured using a Metrohm® combined electrode calibrated at temperatures ranging from +1 °C to +4 °C on the total hydrogen ion scale using TRIS (2-amino-2hydroxymethyl-1.3-propanediol) and AMP (2-aminopyridine) buffers prepared at salinities of 35 and 75 according to the formulations proposed by *Department of Energy (DOE)* [1994]. The pH measurements were carried out at below +4 °C. The accuracy of pH measurements was ± 0.01 pH units [*Frankignoulle and Borges*, 2001]. TA was measured by open-cell titration with HCl 0.1 M according to *Gran* [1952] on 50 mL of sea ice melt water samples. Titration was stopped for 10 min at pH 4.2 to ensure that all CaCO$_3$ crystals were dissolved prior to TA measurement over the pH range 3 and 4.2 as required for the Gran function. The accuracy of TA measurements was ± 4 μmol kg^{-1}. Data were quality checked with certified reference material acquired from Andrew Dickson (Scripps Institution of Oceanography, University of California, San Diego). DIC_b and DIC_f were computed from pH and TA_b and TA_f, respectively, according to CO$_2$ acidity constants of *Mehrbach et al.* [1973] refitted by *Dickson and Millero* [1987] and other constants advocated by *DOE* [1994]. We assumed a conservative behavior of CO$_2$ dissociation constants at subzero temperatures because *Delille et al.* [2007] and *Marion* [2001] suggested that thermodynamic constants relevant for the carbonate system can be assumed to be valid at subzero temperatures. DIC_f is not influenced by calcium carbonate dissolution after sampling. DIC_b obtained from TA_b was used for the sake of consistency with the previous work of *Rysgaard et al.* [2007, 2009].

[18] The age of the ice was roughly estimated using the air and sea temperature records from the location of the Barrow Sea Ice Mass Balance Buoy (data available at http://seaice.alaska.edu/gi/data) at the time of the sampling [*Druckenmiller et al.*, 2009]. The time since formation, Δt, was estimated by subtracting the change in the ice thickness, H_i, for each time step until $H_i = 0$ [*Lepparanta*, 1993] according to

$$\Delta H_i = \frac{K_i}{H_i \rho_b L}(T_w - T_a)\Delta t \tag{3}$$

where ρ_b is the sea ice bulk density, K_i the thermal conductivity of the ice, and T_w and T_a the seawater and air temperatures, respectively. The thermal conductivity and the sea ice bulk density were calculated using the formulation as suggested by *Eicken* [2003] and references therein. The latent heat of fusion, L, was kept at 333.9 kJ kg^{-1}. We assumed that T_a and T_w observed at the mass balance site were representative for larger area and that oceanic heat flux was negligible.
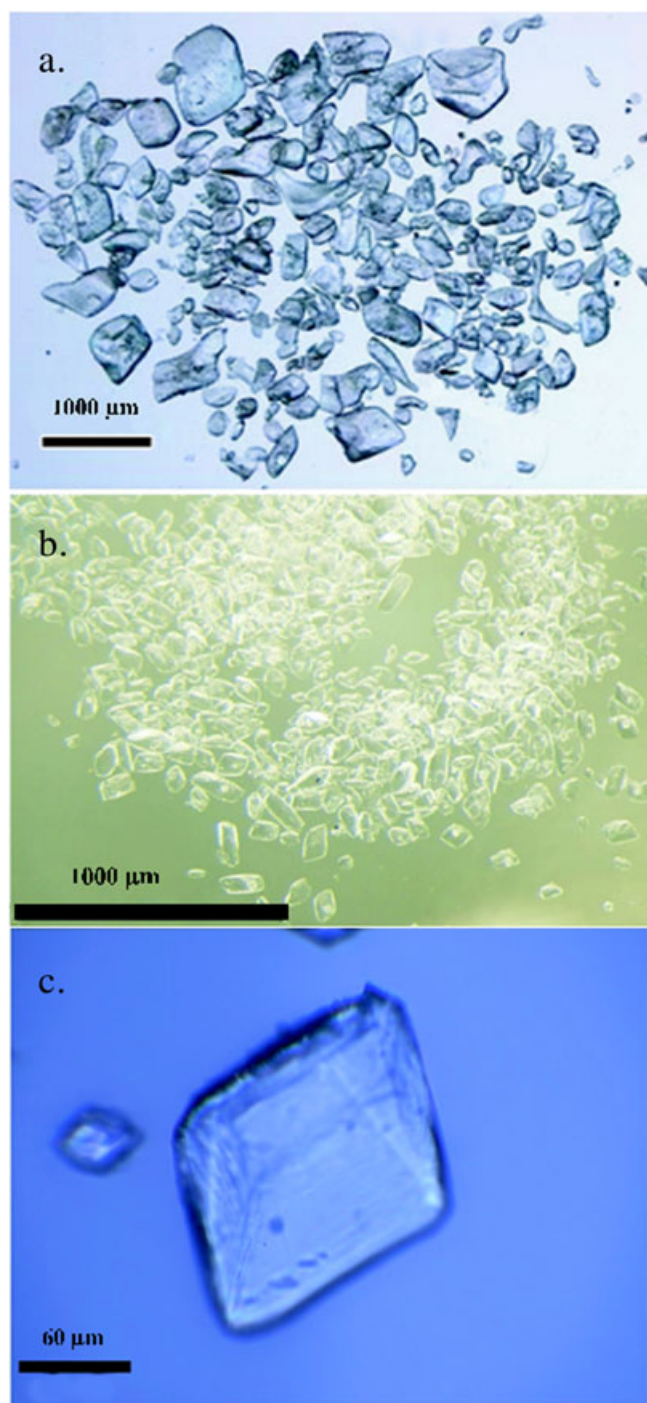
Figure 2. Pictures of ikaite crystals (a) from *Dieckmann et al.* [2008], (b) from our melted sea ice, direct measurement under a binocular microscope, and (c) from a Raman.

3. Results

3.1. Sea Ice Properties

[19] The young sea ice was about 20 cm thick (± 1 cm). A strong temperature gradient was observed between the atmosphere ($T = -23\,°C$), the FF ($T = -19\,°C$) and the sea ice interface with the atmosphere ($T = -14.2\,°C$). The salinity profile was C-shaped, with a salinity of 31.5 at the top of

the ice and 11.2 at the bottom (Figure 3), which is typical for new Arctic sea ice [*Ehn et al.*, 2007]. According to *Golden et al.* [2007], a permeability threshold occurs for a brine volume of 5%. Therefore, this young sea ice was permeable throughout the whole thickness allowing exchanges of matter with the atmosphere or the water column.

[20] A high salinity BS ($S = 114$) covered the ice surface and FF were observed (Figure 4). BS is the result of the upward expulsion of brine associated with sea ice crystal growth and is facilitated by the high porosity within a few centimeters of the surface layer [*Perovich and Richter-Menge*, 1994]. The upper part of the sea ice column was characterized by a distinct layer of fine-grained granular ice (FG) directly followed by a layer of granular ice (G, Figure 4). At 4 cm depth, there was a 2 cm zone of transition between the granular ice and columnar ice (G/C). The rest of the sea ice cover was formed of columnar ice, except at 8 cm depth where a very thin layer (few millimeters) of granular ice was present.

[21] Using T_a and T_w at the mass balance site, equation 3 suggests that sea ice reached the thickness observed at the time of sampling after only 45.5 h. However, the ice was estimated to be 1 week by a local "interpreter" that is consistent with the observed level of frost flower degradation [*Bowman and Deming*, 2010].

3.2. Carbonate System

[22] The pH ranged from 8.7 to 9.5 in the upper layer of young sea ice while FF exhibited a pH of 9.0 (Figure 5a). The pH measured in FF or young sea ice was of the same order of magnitude as observed previously [*Gleitz et al.*, 1995; *Delille et al.*, 2007; *Papadimitriou et al.*, 2007]. TA_f and DIC_f concentration in sea ice ranged from 492 to 863 µmol kg^{-1} melted sea ice and from 418 to 488 µmol kg^{-1} melted sea ice, respectively, while TA_f and DIC_f were much higher in FF
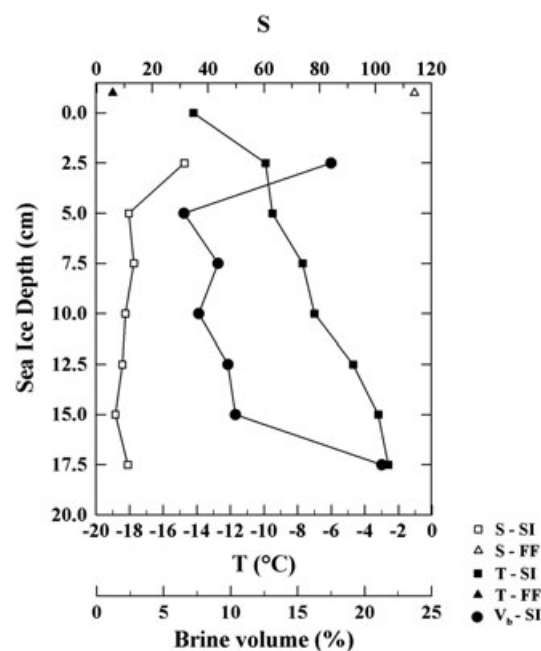

Figure 3. Temperature and salinity and brine volume profile at the Barrow young ice site.
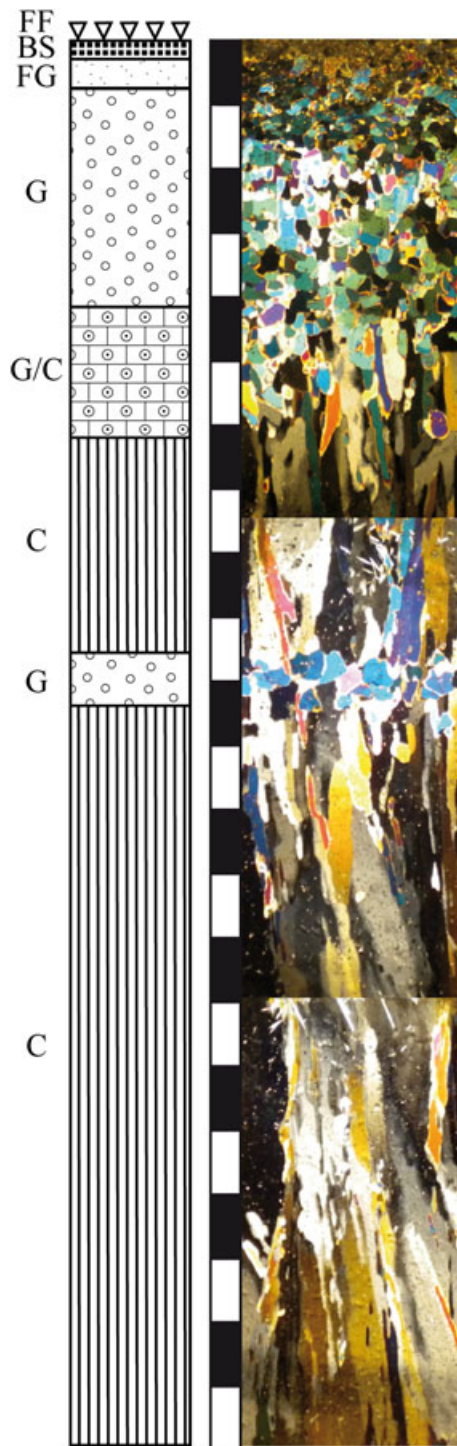
Figure 4. Textural features of the young sea ice include frost flowers (FF), brine skim (BS), fine-grained granular ice (FG), orbicular granular ice (G), intermediate granular/columnar ice (G/C), and columnar ice (C). The black and white scale represents a centimeter scale.

(2586 and 1183 $\mu mol\,kg^{-1}$ melted FF, respectively) (Figure 5b). These results were of the same order of magnitude as the observations of *Rysgaard et al.* [2007, 2009] for Arctic sea ice.

[23] The DIC_f normalized to a salinity of 10 (DIC_{10}, 10 is the mean salinity of this young sea ice) allows us to elucidate

variations in DIC_f (Figure 5c) independent of salinity changes. FF and the upper layer of the young sea ice showed a strong decrease in DIC_{10} value while the rest of the ice column was relatively homogeneous (around 520 $\mu mol\,kg^{-1}$ melted sea ice).

[24] The $TA_b : DIC_b$ ratio in our young sea ice samples ranged from 1.12 to 1.79 in the upper layers with a value peaking at 2.05 in the FF (Figure 5e). According to *Rysgaard et al.* [2007, 2009], a ratio $TA_b : DIC_b$ as high as 2 indicates that calcium carbonate precipitation occurred. This precipitation has been estimated by the difference between the TA_b and TA_f, following the equation 2 to be about 25 $\mu mol\,kg^{-1}$ melted FF in the FF, decreasing from 19.4 $\mu mol\,kg^{-1}$ melted sea ice in the upper part of the ice to 15 $\mu mol\,kg^{-1}$ melted sea ice in the bottom of the ice (Figure 5f). These estimates might be underestimates, as the method does not account for potential $CaCO_3$ dissolution during melting of the ice prior to sub-sampling for TA.

3.3. Air-Ice CO₂ Fluxes

[25] Four measurements of CO_2 fluxes were taken at the sea ice interface with the atmosphere. The fluxes ranged from 4.2 to 9.9 $mmol\,m^{-2}\,d^{-1}$ (positive flux denoting gas evasion), with an overall mean of 6.7 $mmol\,m^{-2}\,d^{-1}$, the magnitudes of which compare reasonably well with values previously reported over sea ice in spring and summer by *Delille* [2006] and *Nomura et al.* [2010a] using the chamber method. However, the fluxes were opposite in direction as, according to *Nomura et al.* [2006], the initial sea ice growth was expected to release CO_2 to the atmosphere.

3.4. Precipitation of Minerals

[26] Various analyses were carried out on crystals found in samples of sea ice melted at +4 °C. Crystals were found at all depths sampled in young sea ice and in FF. First observations under a binocular microscope at room temperature revealed that crystals ranged from <40 μm to 200 μm (Figure 2b). Their morphology was relatively similar to that of the crystals found by *Dieckmann et al.* [2008] but they were significantly smaller. After a few minutes under the binocular, their appearance became milky, a phenomenon also observed by *Whiticar and Suess* [1998] and *Dieckmann et al.* [2010]. This could be due to the transformation of ikaite ($CaCO_3.6H_2O$) into calcite, $CaCO_3$, with increasing crystal temperatures. No clear X-ray diffraction pattern could be obtained from crystals stored on Millipore filters (Figures 6a–6c) even if they had perfect crystal faces. Again, the change of phase as a result of warming during X-ray scanning of the sample may have been responsible for these unidentifiable X-ray patterns. A clear X-ray pattern was finally obtained after leaving the crystals for 1 day at room temperature (Figure 6d); calcite and halite were the two minerals identified by the X-ray scan in this case, as illustrated by the patterns of calcite and halite shown in Figures 6e and 6d. A SEM performed on the same crystals confirmed the presence of calcite, with 84% of the total weight of these crystals in Ca. The Raman spectra of the precipitate and two reference samples (natural calcite and freshly precipitated ikaite) are given in Figure 7. The spectra showed the typical internal vibration modes of the symmetric stretch of the carbonate ion v_1 (1085 cm^{-1} calcite and 1075 cm^{-1} ikaite) and its in-plane band v_4 (715 cm^{-1} calcite
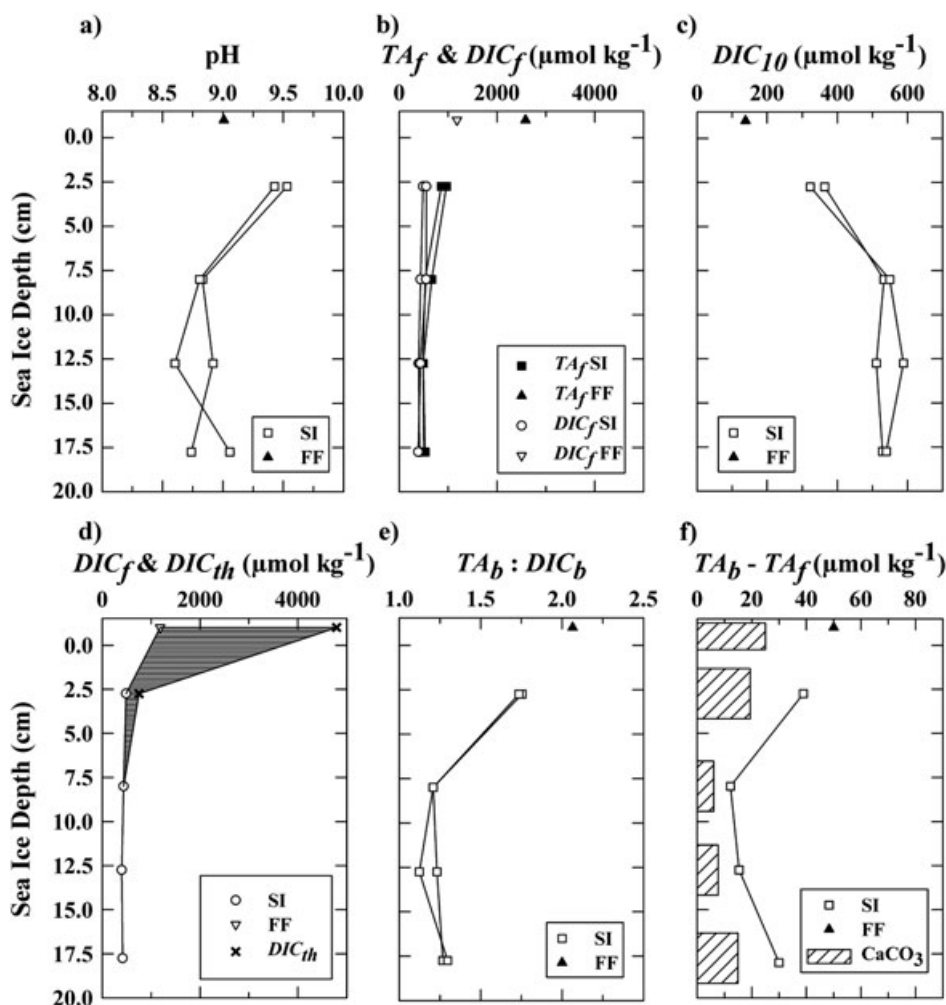
Figure 5. Profiles of (a) pH, (b) TA_f and DIC_f, (c) DIC_{10} (c), (d) difference between the DIC_{th} and DIC_f, (e) ratio between TA_b and DIC_b, and (f) the difference between bulk and filtrated TA with the estimation of the precipitated amount of calcium carbonate.

and 723 cm^{-1} ikaite) [*W. D. Bischoff et al.*, 1985] and the lattice modes in the range between 100 and 300 cm^{-1} were visible. The three duplets at ~150, 200, and 270 cm^{-1} in the ikaite spectra strongly depend on its crystallographic orientation. However, the large difference in the peak positions of the internal modes v_1 and v_4 of calcite and ikaite made it possible to unambiguously distinguish between these two phases. Raman spectra determined on a set of different samples showed ikaite to be the only mineral phase present. These measurements were performed systematically every 5 cm throughout the ice core.

4. Discussion

[27] As sea ice grows, brine expulsion promotes a buildup of a high salinity layer on top of the ice, the BS, allowing several processes to take place. First, it leads to FF formation [*Perovich and Richter-Menge*, 1994; *Alvarez-Aviles et al.*, 2008] and favors direct exchanges with the atmosphere [*Alvarez-Aviles et al.*, 2008; *Bowman and Deming*, 2010]. Second, as the BS concentration increases with the decreasing temperatures, some salts may reach their solubility threshold and start precipitating. Recent studies based on

field observations [*Delille*, 2006; *Delille et al.*, 2007; *Papadimitriou et al.*, 2007; *Dieckmann et al.*, 2008; *Rysgaard et al.*, 2009; *Munro et al.*, 2010] and on laboratory freezing experiments [*Papadimitriou et al.*, 2004; *Nomura et al.*, 2006] indicate that precipitation of CaCO₃ occurs within sea ice. The precipitation of ikaite was found in FF and throughout the sea ice but was not uniformly distributed with depth in the ice cores. Estimations of the amount precipitated, through the $TA_b - TA_f$ difference, showed a C-shape with maxima in the FF (25 μmol kg^{-1} melted FF) and at the bottom (15 μmol kg^{-1} melted sea ice, Figure 5). This shape could be due to the expulsion of salty supersaturated brine from the sea ice to the atmosphere and to the underlying seawater. The $TA_b : DIC_b$ ratio also showed a maximum in the FF. According to *Rysgaard et al.* [2007, 2009], a ratio $TA_b : DIC_b$ as high as 2 indicates the precipitation of calcium carbonate. Our results point out that this precipitation occurs with a lower $TA_b : DIC_b$ ratio and seems to be favored at the surface due to the expulsion of salty supersaturated brine.

[28] Ikaite precipitation in a natural sea ice environment requires several conditions. The saturation state of ikaite is below the saturation at all temperatures in seawater but it
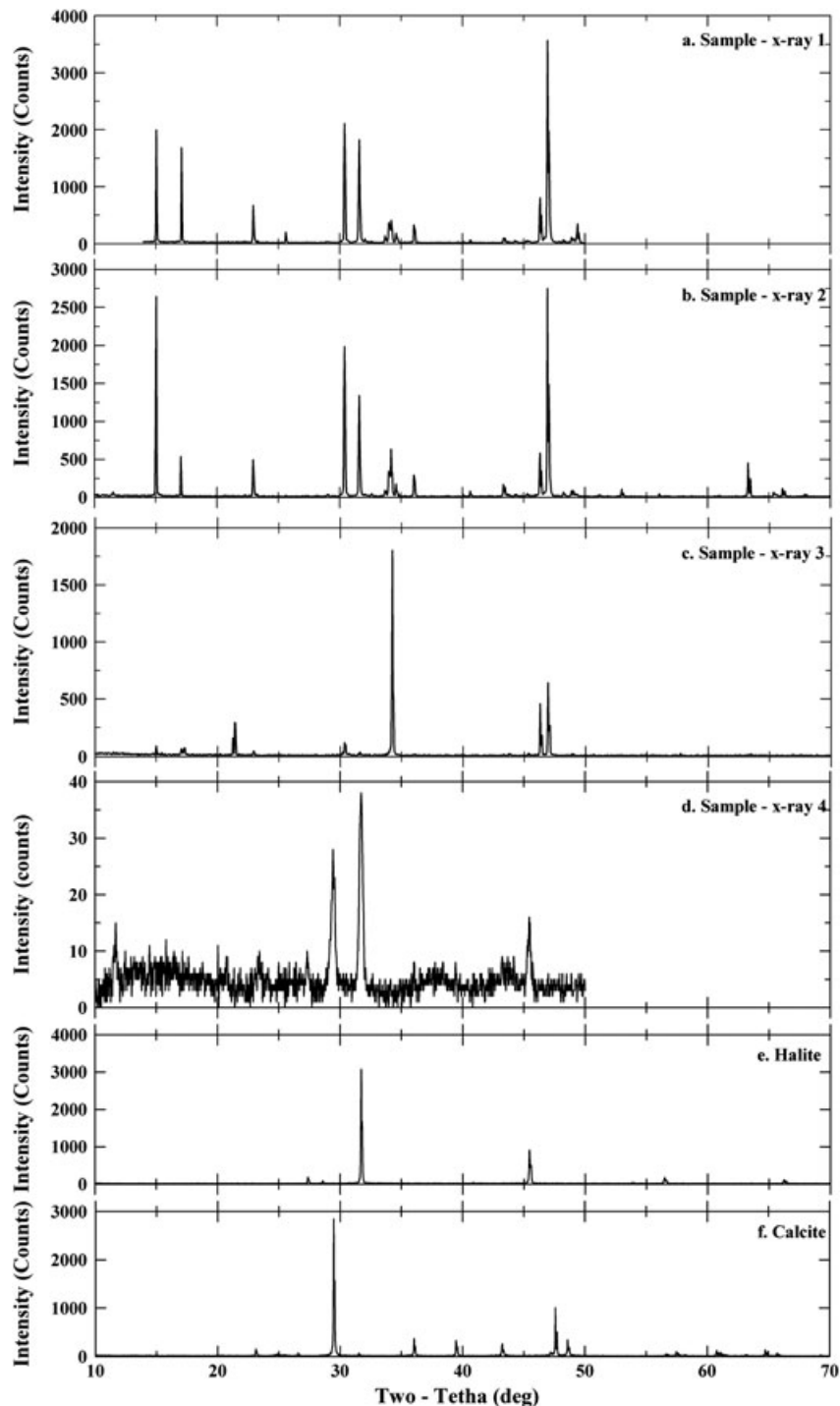
Figure 6. Successive X-ray diffraction patterns of crystals stored on Millipore filters at -25 °C (a–d), X-ray diffraction from same sample after 1 day at room temperature. Line patterns for (e) halite and (f) calcite from the RRUFF database. The database numbers are R070534 for halite and R040070 for calcite.

rapidly approaches saturation near 0 °C. Nevertheless, ikaite cannot form directly by the cooling of seawater [*J. L. Bischoff et al.*, 1993a]. The solution from which it forms must, at least temporarily, be supersaturated with respect to ikaite. This supersaturation is most likely to occur near 0 °C but even then, external additions of either Ca^{2+} or HCO_3^- are required [*J. L. Bischoff et al.*, 1993a]. Furthermore, natural occurrence of ikaite requires conditions which

also inhibit the precipitation of more stable anhydrous forms of $CaCO_3$ [*J. L. Bischoff et al.*, 1993a]. Orthophosphate prevents the crystallization of the more stable anhydrous forms of $CaCO_3$, even at concentrations as low as $5\,\mu M$, but does not interact with ikaite [*J. L. Bischoff et al.*, 1993a; *Buchardt et al.*, 2001]. Accordingly, high PO_4^{3-} concentration gas been linked to ikaite precipitation in Antarctic and Arctic sediments [*Kennedy et al.*, 1987; *Whiticar and*
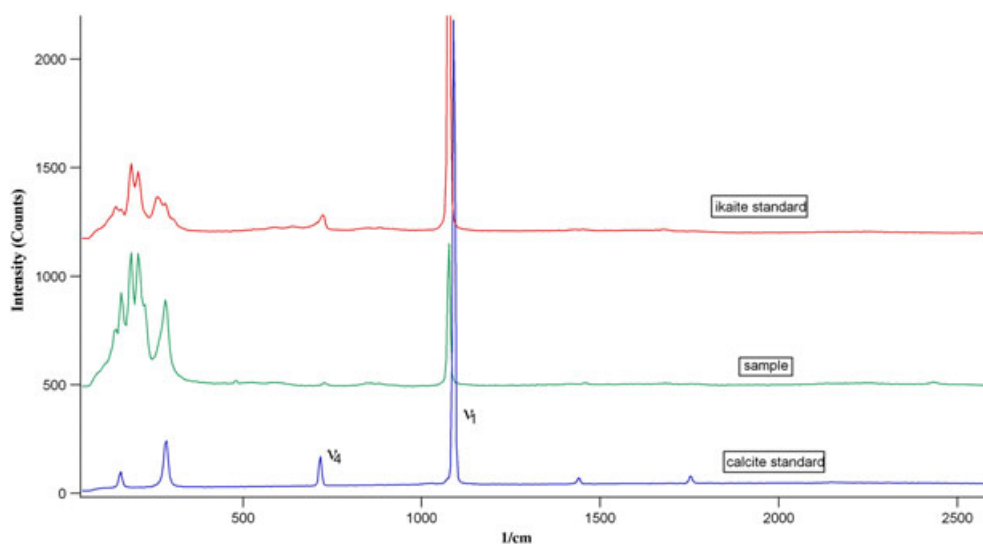
Figure 7. Raman spectra of calcite standard (blue), ikaite (red), and sample (green).

Suess, 1998] and other various environments [*J. L. Bischoff et al.*, 1993b; *Buchardt*, 2004; *Selleck et al.*, 2007]. Hence, ikaite precipitation seems to be favored by near-freezing temperatures, alkaline conditions, elevated phosphate concentrations [*J. L. Bischoff et al.*, 1993a; *Buchardt et al.*, 2001; *Selleck et al.*, 2007], and/or by the presence of certain additives like amino acids [*Whiticar and Suess*, 1998].

[29] With a surface temperature ranging from $-9.9\,°C$ to $-14\,°C$, temperature was not a limiting factor to calcium carbonate precipitation. The phosphate concentration in the ice column ranged from 0.38 to 0.7 μ*M* while the FF concentration was 2.45 μ*M*. These concentrations are comparable with previous studies of Arctic sea ice [*Krembs et al.*, 2002; *Lee et al.*, 2008; *Mathis et al.*, 2009] except for the FF where the PO_4^{3-} concentration is significantly higher. The alkalinity condition was also satisfied at this station with a pH of 9 in the FF. According to *Whiticar and Suess* [1998], the presence of amino acids and phosphates at cold temperatures allows ikaite to form preferentially over calcite or aragonite but this feature is not a universal requirement. *Bowman and Deming*. [2010] collected samples with us (i.e., same day, same sampling site) and measured high concentrations of particulate exopolymeric substances (pEPS) up to 36.5, 725, and 1420 mg gluceq mL^{-1} in melted sea ice, BS, and melted FF, respectively. They pointed out the role of bacterial activity in providing ice-nucleating particles through pEPS production. As suggested by *Whiticar and Suess* [1998], pEPS could also act as calcium carbonate precipitation nuclei; high pEPS production measured in Barrow likely promoted ikaite formation. On the whole, lower temperatures and higher phosphate and pEPS concentration were observed in the BS and FF compared to sea ice, promoting ikaite formation in the surface layers.

[30] Our observations of TA and pH in the top layer of ice in Barrow challenge previous hypothesis by *Sander et al.*, [2006] that significant precipitation of CaCO$_3$ in sea ice and FF significantly reduces the pH buffering capacity of sea ice allowing for a significant decrease in pH. To our best knowledge, pH in sea ice ranges from 7.78 to 9.89

[*Gleitz et al.*, 1995; *Delille et al.*, 2007; *Papadimitriou et al.*, 2007] with a rather elevated higher end value and a much larger range than proposed by *Sander et al.* [2006] (reported range: 2–8).

[31] In both artificial and natural sea ice, a depletion in DIC was observed in sea ice brine [*Papadimitriou et al.*, 2004] and in the ice [*Munro et al.*, 2010] that could not be ascribed to biological activity. In both cases, the authors suggest that CaCO$_3$ precipitation and CO$_2$ degassing may occur in sea ice without being able to elucidate the processes by which these phenomena occur. We observed a strong decrease of the DIC_{10} in the upper layer of the ice column and in the FF. We attempt to assess the overall depletion in the upper layer by assuming that DIC_{10} should be homogeneous over the ice column as should be the case if no biogeochemical processes occur (i.e., primary production, CaCO$_3$ precipitation, and CO$_2$ transfer to the gas phase). We then take into account DIC_f at 7.5 cm ($DIC_{7.5cm}$ and compute DIC_{th} as the value of $DIC_{7.5cm}$ extrapolated to the salinity encountered in the upper part of the ice column assuming a linear relationship between DIC and salinity). DIC_{th} at a given depth *i* was then computed according to

$$DIC_{th} = \frac{DIC_{7.5\,cm} \times S_i}{S_{7.5\,cm}} \qquad (4)$$

where $DIC_{7.5cm}$ is the DIC at 7.5 cm, $S_{7.5cm}$ and S_i are the salinities at 7.5 cm and at a given depth *i*, respectively. The difference between the DIC_f (Figure 5d) and the DIC_{th} represents the loss of DIC, illustrated by the hatched area in Figure 5d. This loss is estimated to be 2069 μmol kg^{-1} melted sample, from the FF down to 7.5 cm depth. Only a few studies estimate the primary production in Arctic sea ice and the results range widely, from 0.03 to 463 mg C m^{-2} d^{-1} [*Arrigo et al.*, 2010]. *Gosselin et al.* [1997] reported a rate of production of 47 mg C m^{-2} d^{-1} in an area between 70°N–75°N and 169°W–170°W during Arctic summer. Considering an ice thickness of 1 m, this production is about 19.6 μmol C kg^{-1} d^{-1}. Applying this rate to an ice cover of 20 cm during 7 days, we found a production of 19.6 μmol C kg^{-1} d^{-1}. Integrated for

7 days, this yields production of 137 µmol C kg^{-1}, which corresponds to only 6.7% of the DIC depletion observed. This is probably an overestimate as *Arrigo and Sullivan* [1992] found greatly reduced photosynthetic rates in fast ice at brine salinities higher than 50 and total photosynthetic shutdown at brine salinity higher than 100, which is the range of salinity found at this station within the upper 10 cm of ice. According to the amount of calcium carbonate precipitated in the FF (25 µmol kg^{-1} melted FF) and in the top 10 cm of the ice (19 + 6 µmol kg^{-1} melted sea ice), the CO$_2$ generated by this precipitation corresponds only to 50 µmol kg^{-1} of melted sample. The part of the precipitation process in the release of CO$_2$ from the BS and/or FF is therefore minor compared to the total exchanges of 2069 µmol kg^{-1} melted sample estimated from the DIC depletion. In the same way *Munro et al.* [2010] used $\delta^{13}C_{DIC}$ to determine the fractional contributions of CaCO$_3$ precipitation and CO$_2$ degassing. They found that degassing seems to be solely responsible for DIC depletion. Therefore, we consider that the contribution of primary production and calcium carbonate precipitation to DIC depletion are negligible, at least near the top of the ice. DIC depletion then mainly corresponds to a release of CO$_2$ from the ice to the atmosphere during the upward expulsion of brine supersaturated in CO$_2$. According to several studies [*Rankin et al.*, 2000; 2002; *Alvarez-Aviles et al.*, 2008; *Bowman and Deming*, 2010], FF and BS facilitate salt transport (or other materials) to the atmosphere and frost flowers increase the specific surface area of the ice of about 40% [*Domine et al.*, 2005]. Also, enhanced salt transport, related brine concentration, and increase of specific surface area potentially promote CO$_2$ degassing.

[32] Our results indicate that DIC loss in the top 7.5 cm of the ice was 2069 µmol kg^{-1} melted sample. Considering a mean sea ice density of 910 kg m^{-3} [*Timco and Frederking*, 1996], the mass of the top 7.5 cm of ice in direct interaction with the atmosphere is estimated to be 68 kg per square meter of ice. Therefore, 1 m^2 of ice loses about 141.2 mmol kg^{-1} of DIC. If the ice is between 2 and 7 days old, this loss of DIC would correspond to a CO$_2$ flux ranging from 20 to 40 mmol m^{-2} d^{-1}. This efflux is approximately four times larger than CO$_2$ flux measured with the chamber method during our relatively short sampling period, which ranged from 4.2 to 9.9 mmol m^{-2} d^{-1}. Air-ice CO$_2$ fluxes are modulated by ice permeability (linked to sea ice porosity), but also snow permeability and air-ice pCO$_2$ gradients. These parameters are likely to evolve rapidly during sea ice growth, together with temperature and bulk salinity for permeability [*Golden et al.*, 2007], and brine concentration and air-ice CO$_2$ exchanges [*Delille*, 2006; *Delille et al.*, 2007; *Nomura et al.*, 2010b; *Geilfus et al.*, 2012] for air-ice pCO$_2$ gradients. The CO$_2$ fluxes measurements provided by the chamber method only provide a snapshot that does not account for past processes, while the CO$_2$ deficit method accounts for the overall CO$_2$ release of the past days, probably right from the beginning of the ice formation. The deficit method presented above is therefore a more robust method than chamber measurements in providing a budget of air-ice CO$_2$ fluxes integrated over the time.

5. Conclusions

[33] Raman and X-ray analyses of thin shore fast ice and FF collected in Barrow, Alaska, show conspicuous evidence of calcium carbonate precipitation as ikaite in the FF and throughout the ice. Precipitation of ikaite in sea ice is not yet fully understood. Ikaite precipitation seems to be favored by near-freezing temperatures, alkaline conditions, elevated phosphate concentrations, and/or by the presence of certain additives like amino acids [*J. L. Bischoff et al.*, 1993a; *Whiticar and Suess*, 1998; *Buchardt et al.*, 2001; *Selleck et al.*, 2007]. Our results suggest that all these conditions were satisfied at our sampling location. In addition, the role of sea ice as a trigger for tropospheric ozone depletion as a consequence of low pH due to CaCO$_3$ precipitation and related reduced sea ice buffer capacity should be considered with caution. Investigations are needed to further understand and budget ikaite precipitation in sea ice.

[34] According to the amount of CaCO$_3$ precipitated in FF and in the upper layer of the ice (top 10 cm), the amount of CO$_2$ generated by this process is therefore minor compared to the total flux estimated by DIC depletion. This decrease of 2069 µmol kg^{-1} melted sample mainly corresponds to a release of CO$_2$ from the ice to the atmosphere due to expulsion of brine supersaturated in CO$_2$. If the ice was between 2 and 7 days old, the loss in DIC corresponded to a CO$_2$ flux ranging from 20 to 40 mmol m^{-2} d^{-1}.

[35] The air-sea ice CO$_2$ fluxes derived from the DIC depletion are large compared to the overall amount of DIC within the ice. If we compare the DIC deficit of the ice (2069 µmol kg^{-1} melted sample) to the DIC concentration of the underlying seawater (2230 µmol kg^{-1}), about 92% of the DIC in the top 7.5 cm of the ice is rejected into the atmosphere. This is not surprising since it is well documented that the ice rejects more than two third of its salt, mainly to the underlying water. However, during our survey of the first stage of sea ice growth, the formation of frost flowers indicated an upward rejection of brine at the air-ice interface. While most of the salts remain at the surface of the ice, gases mix with the atmosphere and are therefore effectively removed from the ice. This explains why gases are more efficiently expelled from the ice compared to salts in the case of upward brine expulsion during the first stage of sea ice formation and is consistent with the observations of *Loose et al.* [2009] who show enhanced rejection of gas (O$_2$) compared to salt. Brine expulsion appears to support significant release of CO$_2$ from the top of polar ocean waters to the atmosphere during the first stages of sea ice growth. This leads to a significant depletion in DIC of the top centimeters of the ice.

References

Alvarez-Aviles, L., W. R. Simpson, T. A. Douglas, M. Sturm, D. Perovich, and F. Domine (2008), Frost flower chemical composition during growth and its implications for aerosol production and bromine activation, *J. Geophys. Res.*, 113, D21304, doi: 10.1029/2008JD010277.

Arrigo, K. R., and C. W. Sullivan (1992), The influence of salinity and temperature covariation on the photophysiological characteristics of Antarctic sea ice microalgae, *J. Phycol.*, 28(6), 746–756.

Arrigo, K. R., T. Mock, and P. M. Lizotte (2010), Primary producers and sea ice, in Sea Ice, 2nd *edition*, Blackwell Sci., London, pp. 283–326, Oxford.

Assur, A. (1958), Composition of sea ice and its tensile strength, in Arctic Sea Ice, edited by National Academy of Sciences–National Research Council. Easton, Maryland.

Bates, N. R., and J. T. Mathis (2009), The Arctic Ocean marine carbon cycle: Evaluation of air-sea CO₂ exchanges, ocean acidification impacts and potential feedbacks, *Biogeosciences*, 6(11), 2433–2459.

Bischoff, J. L., J. A. Fitzpatrick, and R. J. Rosenbauer (1993a), The solubility and stabilization of ikaite (CaCO₃.6H₂O) from 0 °C to 25 °C environmental and paleoclimatic implications for Thinolite Tufa, *J. Geol.*, 101(1), 21–33.

Bischoff, J. L., S. Stine, R. J. Rosenbauer, J. A. Fitzpatrick, and T. W. Stafford (1993b), Ikaite precipitation by mixing of shoreline springs and lake water, Mono Lake, California, USA, *Geochimica Et Cosmochimica Acta*, 57(16), 3855–3865.

Bischoff, W. D., S. K. Sharma, and F. T. Mackenzie (1985), Carbonate ion disorder in synthetic and biogenic magnesian calcites: A Raman spectral study, *American Mineralogist*, 70, 581–589.

Bowman, J. S., and J. W. Deming (2010), Elevated bacterial abundance and exopolymers in saline frost flowers and implications for atmospheric chemistry and microbial dispersal, *Geophys. Res. Lett.*, 37, L13501, doi: 10.1029/2010GL043020.

Buchardt, B. (2004), Ikaite geochemistry and formation of submarine tufas in Greenland, *Geochimica Et Cosmochimica Acta*, 68(11), A348–A348.

Buchardt, B., C. Israelson, P. Seaman, and G. Stockmann (2001), Ikaite tufa towers in Ikka Fjord, southwest Greenland: Their formation by mixing of seawater and alkaline spring water, *J. Sediment. Res.*, 71(1), 176–189.

Delille, B. (2006), Inorganic carbon dynamics and air-ice-sea CO₂ fluxes in the open and coastal waters of the Southern Ocean, 296 pp, Université de Liège, Liège.

Delille, B., B. Jourdain, A. V. Borges, J. L. Tison, and D. Delille (2007), Biogas (CO₂, O-2, dimethylsulfide) dynamics in spring Antarctic fast ice, *Limnology and Oceanography*, 52(4), 1367–1379.

Deming, J. W. (2010), Sea ice bacteria and viruses, in Sea Ice, 2nd *ed*, edited by D. N. Thomas and G. S. Dieckmann, pp. 1–22, Wiley-Blackwell, Oxford.

Dickson, A. G., and F. J. Millero (1987), A comparison of the equilibrium constants for the dissociation of carbonic acid in seawater media, *Deep Sea Research*, I(34), 1733–1743.

Dieckmann, G. S., G. Nehrke, C. Uhlig, J. Göttlicher, S. Gerland, M. A. Granskog, and D. N. Thomas (2010), Brief communication: Ikaite (CaCO₃.6H₂O) discovered in Arctic sea ice, *The Cryosphere*, 4, 227–230.

Dieckmann, G. S., G. Nehrke, S. Papadimitriou, J. Gottlicher, R. Steininger, H. Kennedy, D. Wolf-Gladrow, and D. N. Thomas (2008), Calcium carbonate as ikaite crystals in Antarctic sea ice, *Geophys. Res. Lett.*, 35, L08501, doi: 10.1029/2008GL033540.

DOE (U.S. Department of Energy) (1994), Handbook of Methods for the Analysis of the Various Parameters of the Carbon Dioxide System in Sea Water, edited by A. G. Dickson and C. Goyet, Carbon Dioxide Inofrmation Analysis Center, Oak Ridge National Laboratory, Oak Ridge, Tenn.

Domine, F., A. S. Taillandier, and W. R. Simpson (2005), Specific surface area, density and microstructure of frost flowers, *Geophys. Res. Lett.*, 32, L13502, doi: 10.1029/2005GL023245.

Druckenmiller, M. L., H. Eicken, M. A. Johnson, D. J. Pringle, and C. C. Williams (2009), Toward an integrated coastal sea-ice observatory: System components and a case study at Barrow, Alaska, *Cold Regions Science and Technology*, 56(2-3), 61–72.

Ehn, J. K., B. J. Hwang, R. Galley, and D. G. Barber (2007), Investigations of newly formed sea ice in the Cape Bathurst polynya: 1. Structural, physical, and optical properties, *J. Geophys. Res. Oceans*, 112, CO5002, doi: 10.1029/2006JC003702.

Eicken, H. (2003), From the microscopic to the macroscopic to the regional scale, growth, microstrucutre and properties of sea ice, in Sea Ice—An Introduction to its Physics, Biology, Chemistry and Geology, edited by D. N Thomas and G. S Dieckmann, pp. 22–81, Wiley-Blackwell, Hoboken, N. J.

Frankignoulle, M. (1988), Field-measurements of air sea CO₂ exchange, *Limnology and Oceanography*, 33(3), 313–322.

Frankignoulle, M., and A. V. Borges (2001), Direct and indirect pCO₂ measurements in a wide range of pCO₂ and salinity values (the Scheldt estuary), *Aquatic Geochemistry*, 7(4), 267–273.

Geilfus, N. X., G. Carnat, T. N. Papakyriakou, J. L. Tison, B. Else, H. Thomas, E. H. Shadwick, and B. Delille (2012), pCO2 dynamics and related air-ice CO2 fluxes in the Arctic coastal zone (Amundsen Gulf,

Beaufort Sea), *J. Geophys. Res.*, 117, C00G10, doi: 10.1029/2011JC007118.

Gleitz, M., M. R. v.d. Loeff, D. N. Thomas, G. S. Dieckmann, and F. J. Millero (1995), Comparison of summer and winter in organic carbon, oxygen and nutrient concentrations in Antarctic sea ice brine, *Mar. Chem.*, 51(2), 81–91.

Golden, K. M., H. Eicken, A. L. Heaton, J. Miner, D. J. Pringle, and J. Zhu (2007), Thermal evolution of permeability and microstructure in sea ice, *Geophysical Research Letters*, 34, L16501, doi: 10.1029/2007GL030447.

Gosselin, M., M. Levasseur, P. A. Wheeler, R. A. Horner, and B. C. Booth (1997), New measurements of phytoplankton and ice algal production in the Arctic Ocean, *Deep Sea Research II*, 44(8), 1623–1644.

Gran, G. (1952), Determination of the equivalence point in potentiometric titration, *Analyst, Part II*(77), 661–671.

Grasshoff, K., M. Ehrhardt, and K. Kremling (1983), Methods of Seawater Analysis, 2nd ed., 419 pp., Verlag Chemie, New York.

Kennedy, G. L., D. M. Hopkins, and W. J. Pickthorn (1987), Ikaite, the glendonite precursor, in estuarine sediments at Barrow, Arctic Alaska, *Geological Survey of Alaska Annual Meeting, Abstract, Programme 9*, 725.

Krembs, C., H. Eicken, K. Junge, and J. W. Deming (2002), High concentrations of exopolymeric substances in Arctic winter sea ice: Implications for the polar ocean carbon cycle and cryoprotection of diatoms, *Deep-Sea Research Part I-Oceanographic Research Papers*, 49(12), 2163–2181.

Lee, S. H., T. E. Whitledge, and S. H. Kang (2008), Spring time production of bottom ice algae in the landfast sea ice zone at Barrow, Alaska, *J. Exp. Mar. Biol. Ecol.*, 367(2), 204–212.

Lepparanta, M. (1993), A review of analytical models of sea-ice growth, *Atmos.-Ocean*, 31(1), 123–138.

Loose, B., W. R. McGillis, P. Schlosser, D. Perovich, and T. Takahashi (2009), Effects of freezing, growth, and ice cover on gas transport processes in laboratory seawater experiments, *Geophys. Res. Lett.*, 36(5), L05603 doi: 10.1029/2008GL036318.

Marion, G. M. (2001), Carbonate mineral solubility at low temperatures in the Na-K-Mg-Ca-H-Cl-SO₄-OH-HCO₃-CO₃-CO₂-H₂O system, *Geochimica Et Cosmochimica Acta*, 65(12), 1883–1896.

Mathis, J. T., N. R. Bates, D. A. Hansell, and T. Babila (2009), Net community production in the northeastern Chukchi Sea, *Deep-Sea Research Part II-Topical Studies in Oceanography*, 56(17), 1213–1222.

Mehrbach, C., C. H. Culberson, J. E. Hawley, and R. M. Pytkowicz (1973), Measurements of the apparent dissociation constants of carbonic acid in seawater at atmospheric pressure, *Limnology and Oceanography*, 18, 897–907.

Miller, L., T. Papakyriakou, R. E. Collins, J. Deming, J. Ehn, R. W. Macdonald, A. Mucci, O. Owens, M. Raudsepp, and N. Sutherland (2011), Carbon dynamics in sea ice: A winter flux time series, *J. Geophys. Res. Oceans*, 116, C02028, doi: 10.1029/2009JC006058.

Morin, S., G. M. Marion, R. von Glasow, D. Voisin, J. Bouchez, and J. Savarino (2008), Precipitation of salts in freezing seawater and ozone depletion events: A status report, *Atmos. Chem. Phys.*, 8(23), 7317–7324.

Munro, D. R., R. B. Dunbar, D. A. Mucciarone, K. R. Arrigo, and M. C. Long (2010), Stable isotope composition of dissolved inorganic carbon and particulate organic carbon in sea ice from the Ross Sea, Antarctica, *J. Geophys. Res. Oceans*, 115, C09005, doi: 10.1029/2009JC005661.

Nomura, D., H. Yoshikawa-Inoue, and T. Toyota (2006), The effect of sea-ice growth on air-sea CO₂ flux in a tank experiment, *Tellus Series B-Chemical and Physical Meteorology*, 58(5), 418–426.

Nomura, D., H. Yoshikawa-Inoue, T. Toyota, and K. Shirasawa (2010a), Effects of snow, snow-melting and re-freezing processes on air-sea ice CO₂ flux, *J. Glaciology*, 56(196), 262–270.

Nomura, D., H. Eicken, R. Gradinger, and K. Shirasawa (2010b), Rapid physically driven inversion of the air-sea ice CO₂ flux in the seasonal landfast ice off Barrow, Alaska after onset surface melt, *Continental Shelf Research*, 30(19), 1998–2004.

Papadimitriou, S., H. Kennedy, G. Kattner, G. S. Dieckmann, and D. N. Thomas (2004), Experimental evidence for carbonate precipitation and CO₂ degassing during sea ice formation, *Geochimica et Cosmochimica Acta*, 68(8), 1749–1761.

Papadimitriou, S., D. N. Thomas, H. Kennedy, C. Haas, H. Kuosa, A. Krell, and G. S. Dieckmann (2007), Biogeochemical composition of natural sea ice brines from the Weddell Sea during early austral summer, *Limnology and Oceanography*, 52(5), 1809–1823.

Papakyriakou, T., and L. Miller (2011), Springtime CO₂ exchange over seasonal sea ice in the Canadian Arctic Archipelago, *Annals of Glaciology*, 52, 215–224.

Perovich, D. K., and J. A. Richter-Menge (1994), Surface characteristics of lead ice, *Journal of Geophysical Research-Oceans*, 99(C8), 16341–16350.

Piot, M., and R. von Glasow (2008), The potential importance of frost flowers, recycling on snow, and open leads for ozone depletion events, *Atmos. Chem. Phys.*, 8(9), 2437–2467.

Rankin, A. M., V. Auld, and E. W. Wolff (2000), Frost flowers as a source of fractionated sea salt aerosol in the polar regions, *Geophys. Res. Lett.*, 27(21), 3469–3472.

Rankin, A. M., E. W. Wolff, and S. Martin (2002), Frost flowers: Implications for tropospheric chemistry and ice core interpretation, *J. Geophys. Res.-Atmos.*, *107*(D23), 4683, doi: 10.1029/2002JD002492.

Rysgaard, S., R. N. Glud, M. K. Sejr, J. Bendtsen, and P. B. Christensen (2007), Inorganic carbon transport during sea ice growth and decay: A carbon pump in polar seas, *J. Geophys. Res. Oceans*, *112*, C03016, doi: 10.1029/2006JC003572.

Rysgaard, S., J. Bendtsen, L. T. Pedersen, H. Ramlov, and R. N. Glud (2009), Increased CO$_2$ uptake due to sea ice growth and decay in the Nordic Seas, *J. Geophys. Res.*, *114*(C09011), doi: 10.1029/2008JC005088.

Sander, R., J. Burrows, and L. Kaleschke (2006), Carbonate precipitation in brine—a potential trigger for tropospheric ozone depletion events, *Atmos. Chem. Phys.*, *6*, 4653–4658.

Selleck, B. W., P. F. Carr, and B. G. Jones (2007), A review and synthesis of glendonites (pseudomorphs after ikaite) with new data: Assessing applicability as recorders of ancient coldwater conditions, *J. Sediment. Res.*, *77*(11), 980–991.

Semiletov, I. P., A. Makshtas, S. I. Akasofu, and E. L. Andreas (2004), Atmospheric CO$_2$ balance: The role of Arctic sea ice, *Geophys. Res. Lett.*, *31*, L05121, doi: 10.1029/2003GL017996.

Semiletov, I. P., I. Pipko, I. Repina, and N. E. Shakhova (2007), Carbonate chemistry dynamics and carbon dioxide fluxes across the atmosphere-ice-water interfaces in the Arctic Ocean: Pacific sector of the Arctic, *J. Mar. Syst.*, *66*(1-4), 204–226.

Takahashi, T., *et al.* (2009), Climatological mean and decadal change in surface ocean pCO$_2$, and net sea-air CO$_2$ flux over the global oceans, *Deep-Sea Research Part II-Topical Studies in Oceanography*, *56*(8-10), 554–577.

Thomas, D. N., S. Papadimitriou, and C. Michel (2010), Biogeochemistry of sea ice, in Sea Ice, 2nd *ed.*, edited by D. N. Thomas and G. S. Dieckmann, p. 621, Wiley-Blackwell, Hoboken, N. J.

Timco, G. W., and R. M. W. Frederking (1996), A review of sea ice density, *Cold Regions Science and Technology*, *24*(1), 1–6.

Tison, J. L., A. Worby, B. Delille, F. Brabant, S. Papadimitriou, D. Thomas, J. de Jong, D. Lannuzel, and C. Haas (2008), Temporal evolution of decaying summer first-year sea ice in the Western Weddell Sea, Antarctica, *Deep-Sea Research Part II-Topical Studies in Oceanography*, *55*(8-9), 975–987.

Weeks, W. F., and S. F. Ackley (1982), The growth, structure, and properties of sea ice., 117 pp., CRREL Monograph.

Whiticar, M. J., and E. Suess (1998), The cold carbonate connection between Mono Lake, California and the Bransfield Strait, Antarctica, *Aquatic Geochemistry*, *4*(3-4), 429–454.

Zemmelink, H. J., B. Delille, J. L. Tison, E. J. Hintsa, L. Houghton, and J. W. H. Dacey (2006), CO$_2$ deposition over the multi-year ice of the western Weddell Sea, *Geophys. Res. Lett.*, *33*, L13606, doi: 10.1029/2006GL026320.